Energy Proceedings
Vol 38, 2024
ISSN 2004-2965

Multi-Phase and Multi-Species Transport Inside Air-Breathing Photocathode of Photocatalytic Fuel Cell

Wei Zhang [1,2], Youxu Yu [1,2], Yuxin Liu [1,2], Xun Zhu [1,2], Dingding Ye [1,2], Yang Yang [1,2], Hong Wang [1,2], Rui Wu [3], Rong Chen [1,2]*, Qiang Liao [1,2]

1 Key Laboratory of Low-Grade Energy Utilization Technologies and Systems (Chongqing University), Ministry of Education, Chongqing 400030, China;

2 Institute of Engineering Thermophysics, School of Energy and Power Engineering, Chongqing University, Chongqing 400030, China;

3 School of Mechanical Engineering, Shanghai Jiao Tong University, Shanghai 200240, China
(*Corresponding Author: rchen@cqu.edu.cn)

ABSTRACT

A deep understanding of the two-phase and multi-species transport coupled with photoelectrochemical oxygen reduction reaction is crucial for boosting a photocatalytic fuel cell with a photoanode and an air-breathing photocathode. Herein, a pore network model is developed for the air-breathing CuO photocathode employed in photocatalytic fuel cell to describe the two-phase percolation and multi-species transport as well as their effect on the photocathode performance. The performance of the air-breathing photocathode is found to be greatly affected by the wettability-dependent liquid invasion into the gas diffusion layer. Increasing the proportion of hydrophilic pores/throats in the gas diffusion layer greatly lowers the photocathode performance because of more severe liquid invasion. Besides, the transport of active species, including the dissolved oxygen and photo-excited electron and hole, has a significant effect on the photocathode performance. The present work also provides a guidance for the optimal design of the air-breathing photocathode.

Keywords: pore network model, two-phase percolation, multi-species transport, air-breathing photocathode, photocatalytic fuel cell

1. INTRODUCTION

Featured with degrading organic pollutants and simultaneously recovering the stored chemical energy into electricity by the use of solar energy, photocatalytic fuel cell (PFC) has been considered as a promising technology in environment and energy applications [1]. A PFC is typically composed of a photoanode, a cathode, and an electrolyte mixed with organic pollutants. The cathode is a key component affecting the PFC performance. Noble metals are usually employed as the cathode catalysts [2], whose high cost impedes the large-scale PFC application. Therefore, extensive efforts have also been paid to the development of photocathode to replace the noble-metal cathode catalysts. Copper oxide (CuO) has been considered as a promising semiconductor for the photocathode because of good stability and solar response [3, 4]. The transport of oxidant (oxygen) is also critically important for the photocathode performance. In conventional PFCs, the required oxygen is usually dissolved in the electrolyte [5]. The photocathode performance is tremendously limited by extremely low solubility of oxygen and sluggish diffusion of dissolved oxygen. In order to enhance the oxygen transport, an air-breathing CuO photocathode was developed and successfully applied in the PFC [6]. Although the oxygen transport was enhanced by this design, the photocurrent is still much below the limiting photocurrent (AM 1.5, 35 mA/cm^2 [3]). One of possible reasons lies in the limited transport of active species. Therefore, a deep understanding of the multi-species transport characteristics coupled with photoelectrochemical reactions at the photocathode is essential.

Typically, the air-breathing photocathode is composed of a porous gas diffusion layer (GDL) and a porous photocatalytic layer (PL). The porous PL is in contact with the liquid electrolyte to ensure large active surface area for photoelectrochemical reactions, and the

This is a paper for 15th International Conference on Applied Energy (ICAE2023), Dec. 3-7, 2023, Doha, Qatar.

porous GDL is hydrophobically treated to ensure efficient oxygen transfer and avoid the liquid leakage. During the operation, however, there is still some liquid electrolyte that can penetrate into the porous GDL, occupying the pore space and thereby lowering the oxygen transfer [7]. Thus, an insight into the characteristics of the two-phase mass transfer is essential for better design of the air-breathing photocathode. Numerical simulation offers a preferable approach to shed light into the two-phase mass transport. Conventional numerical studies usually adopt homogeneous models, but the liquid electrolyte percolation inside the porous photocathode controlled by the capillary action is hard to precisely described [8]. This issue can be addressed by mesoscopic simulation approaches. Among the mesoscopic approaches [9-11], the pore network model (PNM) with the benefits of time-saving has been successfully applied to the investigation of mass transport inside the porous electrode [11,12]. Wu et al. [11] simulated the gas phase displacement process in the porous medium by the PNM; the simulation results were in good agreement with the experimental data, indicating the feasibility of the PNM to simulate the two-phase percolation in the porous medium. Although numerous works on the PNM have been carried out for the porous electrodes in fuel cells, the numerical investigation on the transport characteristics of the active species coupling with the liquid electrolyte percolation and the photoelectrochemical reaction via the pore network model has not been reported yet, limiting the optimization of the air-breathing photocathode. Herein, a pore network model describing the two-phase percolation, multiple species transport coupled with the photoelectrochemical reaction is developed for the air-breathing photocathode to reveal the two-phase and multiple species transport. Moreover, the effects of the mixed wettability of the porous GDL are also discussed. The achieved results contribute to not only the deep understanding of transport characteristics but also the optimization of the are-breathing photocathode structure.

2. MODEL DESCRIPTION

2.1 Physical model

In this study, the air-breathing photocathode is composed of randomly packed CuO nanoparticles serving as the porous photocatalytic layer (PL), which are deposited inside the bottom of the porous carbon paper serving as the porous gas diffusion layer (GDL), as shown in Fig. 1a. The air-breathing photocathode is directly opened to the surrounding and the PL is in direct contact with the liquid electrolyte. During the operation, the liquid electrolyte flows over the porous PL, accompanied by the percolation of the liquid electrolyte into the GDL and PL driven by capillary action. While surrounding oxygen in air diffuse through the porous GDL to the PL, and then dissolves in the electrolyte. Meanwhile, electron-hole pairs are excited in the PL after the absorption of incident photons. The photo-excited electrons reduce the dissolved oxygen to complete oxygen reduction reaction, while the photo-excited holes recombine with the electrons from the external circuit. Besides, the recombination of photo-excited holes and photo-excited electrons also occurs.

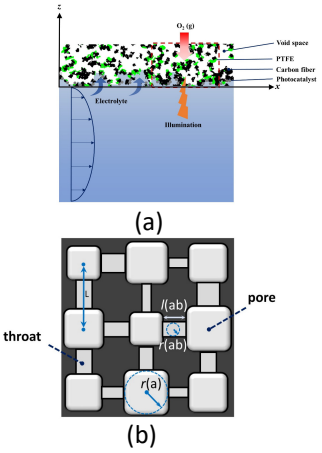

Fig. 1 (a) schematic diagram of the two-dimensional lateral view of the air-breathing photocathode, (b) sectional drawing of the pore network structure.

Considering these above processes, a theoretical model can be developed. Herein, the porous GDL can be represented by the constructed pore network. Typically, the porous GDL fabricated by carbon paper consists of randomly pores, which is hydrophobically treated to avoid the liquid leakage from the air-breathing photocathode. As illustrated in Fig. 1a, the region shown in the dashed box (420×420×210 μm^3) is chosen as the computational domain and a three-dimensional (3D) pore network is developed to represent the pore structure of GDL, the detailed construction of pore network can be found in the previous report [13], and the sectional drawing of the pore network structure is shown in Fig. 1b. As compared to the GDL, the thickness of the PL is much smaller, so that a row of pore at the bottom is used to load the PL, which is hydrophilic to ensure efficient contact between the photocatalysts and liquid electrolyte. The photocatalysts are coated on the walls of the pores at the bottom to form a thin film for the photoelectrochemical oxygen reduction reaction, which can be treated as a homogeneous medium with a rather thin thickness [14]. Therefore, a one-dimensional

mathematical model can be developed for the bottom pores in the pore network to describe the photoelectrochemical reaction and oxygen consumption, whose results will be integrated into the pore network model. Moreover, the results on the two-phase mass transport obtained by the pore network model will be used for solving one-dimensional mathematical model.

2.2 Pore network model

Prior to the model development, some assumptions are made. (i) The air-breathing photocathode is operated under steady state and isothermal condition; (ii) the electrolyte flow in the channel is considered as the Poiseuille flow; (iii) the electrolyte is the dilute solution, whose properties is similar to pure water; (iv) the liquid electrolyte percolation inside the porous media is governed by capillary forces [11], and the liquid pressure gradient in the GDL and PL is negligible; (v) the effect of water consumption by the photoelectrochemical reaction is ignored [10]; (vi) only one phase (liquid phase or gas phase) dominates in a pore or throat; (vii) the transport of electron and hole relies on diffusion [15], and gaseous and dissolved oxygen as well; (viii) when the pore with the photocatalysts is surrounded with liquid phase, the photoelectrochemical reactions occurring in this pore is neglected due to critically high mass transfer resistance of dissolved oxygen. Based on the above assumptions, the model for the air-breathing photocathode is developed.

2.2.1 Liquid percolation in GDL

The invasion percolation algorithm [16] is adopted to simulate the percolation process inside the air-breathing photocathode. The capillary pressure threshold of a pore/throat determines the liquid invasion to the pore/throat, which can be defined according to the Young-Laplace equation [16]. The contact angle of hydrophobic pore/throat and hydrophilic pore/throat are set to be 110° and 80°, respectively [17]. As mentioned, the carbon fiber is usually hydrophobically treated to avoid the liquid leakage. However, it is rather difficult to make all inner surfaces hydrophobic and the mixed wettability is introduced, the proportion of hydrophobic pores/throats is set to 0.8, which is randomly distributed. The pores loaded with photocatalysts and the throats connected with two catalytic pores are considered to be hydrophilic. The gas pressure equals to atmospheric pressure and the liquid pressure is determined by the flowing electrolyte based on the Poiseuille equation [18]. More details of invasion percolation algorithm can be found in ref. [16].

2.2.2 Oxygen transport in the porous GDL

The oxygen transport between pore a and pore b can be given by:

$$q(\mathrm{a,\ b}) = g(\mathrm{a,b})(n_{\mathrm{O_2}}(\mathrm{a}) - n_{\mathrm{O_2}}(\mathrm{b})) \quad (1)$$

where $n_{\mathrm{O_2}}(\mathrm{a})$ denotes the oxygen concentration, $g(\mathrm{a,\ b})$ is the diffusion conductivity between pore a and pore b. The diffusion resistance from pore a to pore b consists of three parts: the resistance from the centroid of pore a to throat ab, the resistance of throat ab and the resistance from throat ab to the centroid of pore b. Thus, the relationship between the diffusion conductivity and the resistance can be obtained:

$$g(\mathrm{a,\ b}) = \left[(0.5g(\mathrm{a}))^{-1} + (g(\mathrm{ab}))^{-1} + (0.5g(\mathrm{b}))^{-1}\right]^{-1} \quad (2)$$

where $g(\mathrm{a})$, $g(\mathrm{b})$ and $g(\mathrm{ab})$ are diffusion conductivities of pore a, pore b and the throat between them. The diffusion conductivity in the pore or throat is determined as:

$$g(\mathrm{a}) = 2\mathrm{D}_{\mathrm{O_2}}^{\mathrm{gas}} r(\mathrm{a}) \quad (3a)$$

$$g(\mathrm{ab}) = 4\mathrm{D}_{\mathrm{O_2}}^{\mathrm{gas}} r(\mathrm{ab})^2 / l(\mathrm{ab}) \quad (3b)$$

where $\mathrm{D}_{\mathrm{O_2}}^{\mathrm{gas}}$ is the bulk diffusion coefficient of oxygen. Since the diffusion of oxygen is much faster than the dissolved oxygen, the oxygen diffusion conductivity of non-catalytic pore and throat invaded by the liquid electrolyte is modified to zero, which is embodied for the transport resistance aroused by the liquid invasion. When the gas phase pore connects with the liquid-phase occupied catalytic pore via the gas phase throat, the diffusion conductivity is modified as:

$$g(\mathrm{a,b}) = \left[(0.5g(\mathrm{a}))^{-1} + (g(\mathrm{ab}))^{-1}\right]^{-1} \quad (4)$$

The oxygen concentration can be obtained by solving the mass conservation equation:

$$\sum_{\mathrm{b}=1}^{n_{\mathrm{a}}} q(\mathrm{a,\ b}) = R(\mathrm{a}) \quad (5)$$

where n_{a} and R_{a} represent the number of vicinal pores and the consumption, respectively. When the pore is the non-catalytic pore, the consumption rate is zero; the consumption rate is calculated based on the local photoelectrochemical reaction rate $V_{\mathrm{re}}(\mathrm{a}, x)$ and the thickness of the thin porous film PL ($\mathrm{L_c}$) in the photocatalytic pore, the distance between two adjacent pore's centroids (L):

$$R_{\mathrm{a}} = \mathrm{L}^2 \int_0^{\mathrm{L_c}} V_{\mathrm{re}}(\mathrm{a}, x)\mathrm{d}x \quad (6)$$

which will be detailed in the following section.

The corresponding boundary conditions are required to solve the above equations. At the outer surface of the porous GDL, the oxygen concentration is considered to be the supplied oxygen concentration; at the inner surface in contact with the liquid electrolyte, the oxygen

flux is zero because of no reaction; The other boundaries are considered as the periodic boundary.

2.2.3 Multi-species transport in thin porous PL

Here, the transport of the multiple species inside the thin porous PL involves dissolved oxygen, excited electron and hole. During the transport process, the dissolved oxygen is reduced by the excited electrons, thus the governing equation of dissolved oxygen is expressed as:

$$D_{O_2}^{eff}\Delta n_{O_2}^{dis}(a, x_c) - V_{re}(a, x_c) = 0 \quad (7)$$

where $n_{O_2}^{dis}(a, x_c)$ represents the local concentration of the dissolved oxygen, $D_{O_2}^{eff}$ represents the effective diffusion coefficient of dissolved oxygen, which can be calculated based on the bulk diffusion coefficient of dissolved oxygen ($D_{O_2}^{dis}$), porosity (ε^c) and the tortuosity (τ^c) of the porous PL.

The photoelectrochemical rate of oxygen reduction reaction can be described as [14]:

$$V_{re}(a, x_c) = k_{re}(n_{e^-}(a, x_c) - n_{int})n_{O_2}^{dis}(a, x_c) \quad (8)$$

where k_{re} represents the rate constant of photoelectrochemical reduction, $n_{e^-}(a, x_c)$ represents the local density of electron, n_{int} is the intrinsic density in CuO.

In addition to the photoelectrochemical oxygen reduction reaction, the transport of the photo-excited electrons and holes, and the recombination of holes and electrons also occur inside the porous PL, which can be described as:

$$D_{e^-}^{eff}\Delta n_{e^-}(a, x_c) + V_{gen}(a, x_c) - V_{rec}(a, x_c) - 4V_{re}(a, x_c) = 0 \quad (9)$$

$$D_{h^+}^{eff}n_{h^+}(a, x_c) + V_{gen}(a, x_c) - V_{rec}(a, x_c) = 0 \quad (10)$$

where $D_{h^+}^{eff}$ and $D_{e^-}^{eff}$ are the effective diffusion coefficient of hole and electron in the porous PL, $n_{h^+}(a, x_c)$ represents the local density of hole, $V_{gen}(a, x_c)$ and $V_{rec}(a, x_c)$ represent the local generation and local recombination rates of photo-excited electron-hole pairs.

The electron-hole generation is achieved by Beer-Lambert law [14]:

$$V_{gen}(a, x_c) = \int_{\lambda_{min}}^{\lambda_{max}} \phi(\lambda)\alpha(\lambda)\exp\left(-\alpha(\lambda)(L_c - x_c)\right) d\lambda \quad (11)$$

where $\phi(\lambda)$ is incident photon flux. Because the photocathode is illuminated from the electrolyte/photocatalyst (E/P) interface, $(L_c - x_c)$ is introduced to correct the local incident photon flux ($\phi(\lambda)$). $\alpha(\lambda)$ represents the absorption coefficient of the PL.

Considering the radiative recombination of photo-excited electron-hole pairs, the local recombination rate can be expressed as [19]:

$$V_{rec}(a, x_c) = k_{rec}\left(n_{e^-}(a, x_c)n_{h^+}(a, x_c) - n_{int}^2\right) \quad (12)$$

where k_{rec} represents the rate constant of recombination.

The corresponding boundary conditions are required to solve the above equations. At the E/P interface, the transport of electron, hole and dissolved oxygen are not allowed. At the photocatalyst/substrate (P/S) interface, the transport of electron is not allowed, the concentrations of dissolved oxygen and hole are calculated based on Henry's law and Fermi distribution, respectively.

The photocathode photocurrent is expressed as:

$$j = \left(\sum_{a=1}^{n_c} j(a)\right)/(L_x L_y) \quad (13)$$

$$j(a) = L^2 q D_{h^+}^{eff}\nabla n_{h^+}(a, 0) \quad (14)$$

where n_c and $j(a)$ represent the number of effective photocatalytic pores and the photocurrent in the photocatalytic pore a; L_x, L_y and q represent the dimensions of the computational domain in *x* and *y* directions, the elementary charge.

2.3 Numerical approach and mesh independence

The solution of the proposed model is realized by implementing the self-written code in MATLAB R2022a and Microsoft Visual Studio 2010. The primary parameters employed are given in Table 1. Before simulation, the mesh independence test is indispensable. The constructed pore network is employed as the photocathode, the thickness, porosity and tortuosity of the porous PL are set to be 5 μm, 0.52, 1.5, respectively. The electrolyte flow in the channel, the illumination intensity (300-800 nm, AM 1.5) and the concentration of supplied oxygen are set to be 200 μL/min, 100 mW/cm^2, 21 % (at atmospheric pressure), respectively. As seen from Fig. 2, when the grid size is 10 nm for the porous PL, the error is smaller than 0.1 %. Therefore, the grid size of 10 nm is chosen in the work.

Table 1 Parameters used in simulation

Parameters	Value	Unit	Reference
$\alpha(\lambda)$		cm^{-1}	[20], UV-Vis spectrum
D_{e^-}	4.56×10^{-7}	$cm^2\,s^{-1}$	[21]
D_{h^+}	1.23×10^{-3}	$cm^2\,s^{-1}$	[22]
D_{O_2}(gas)	0.21	$cm^2\,s^{-1}$	[23]
D_{O_2}(dis)	2.5×10^{-5}	$cm^2\,s^{-1}$	[24]
k_{rec}	7.11×10^{-10}	$cm^3\,s^{-1}$	
k_{re}	4.75×10^{-14}	$cm^3\,s^{-1}$	
n_{int}	1.15×10^{7}	$cm^{-3}\,s^{-1}$	[25-27]

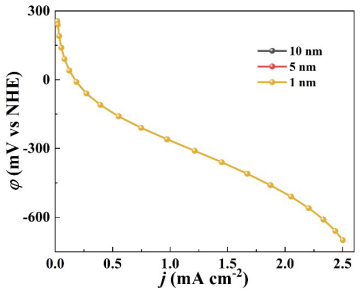

Fig. 2 Results of the mesh independence test.

3. RESULTS AND DISCUSSION

3.1 Two-phase percolation and species transport characteristics

The two-phase percolation and species transport inside the air-breathing photocathode are first presented in this section. In this simulation case, the light intensity (300-800 nm, AM 1.5), the electrolyte concentration and flow rate, the pore radius and porosity of the porous GDL, and the porosity and thickness of the thin porous PL are 100 mW/cm^2, 1.0 M, 200 µL/min, 12.8-17.5 µm, 0.66, 0.52 and 5 µm, respectively. The two-phase percolation highly depends on the distributions of the hydrophobic and hydrophilic pores. Fig. 3a and Fig. 3b show the distributions of hydrophilic pores and the pores filled with liquid electrolyte. As stated earlier, the hydrophilic photocatalysts are loaded in the pores at the bottom of the air-breathing photocathode, making these pores hydrophilic and thus allowing for the liquid electrolyte to invade. The remaining hydrophilic pores are randomly distributed inside the GDL. In this work, the flowable electrolyte makes the pressure difference between the liquid and gas phases lower than the capillary pressure threshold. In this context, the liquid electrolyte can invade those hydrophilic pores. Therefore, the pores invaded by the liquid electrolyte are mostly located near the interface facing the liquid electrolyte. Except the hydrophilic pores adjacent to the bottom hydrophilic pores via the inter-connection of the hydrophilic throats, which can be invaded by the liquid electrolyte, those hydrophilic pores loosely distributed in the porous GDL are still occupied by the gas phase (Fig. 3b). A low liquid saturation in the porous GDL is then resulted, which facilitates the oxygen transport(Fig. 3c). This fact demonstrates that the hydrophobic treatment of the porous GDL cannot only avoid the liquid leakage but also enhance the oxygen transport in the air-breathing photocathode. However, it can also be found that the local oxygen concentrations in some photocatalytic pores are lowered due to the adjacent pores filled by the liquid electrolyte (Fig. 3d), which increases the transfer resistance of oxygen and thereby decreases the local oxygen concentration. Corresponding to the lowered oxygen concentration, the photocurrent densities in these photocatalytic pores are much smaller (Fig. 3e), indicating the inefficiency of these photocatalytic pores.

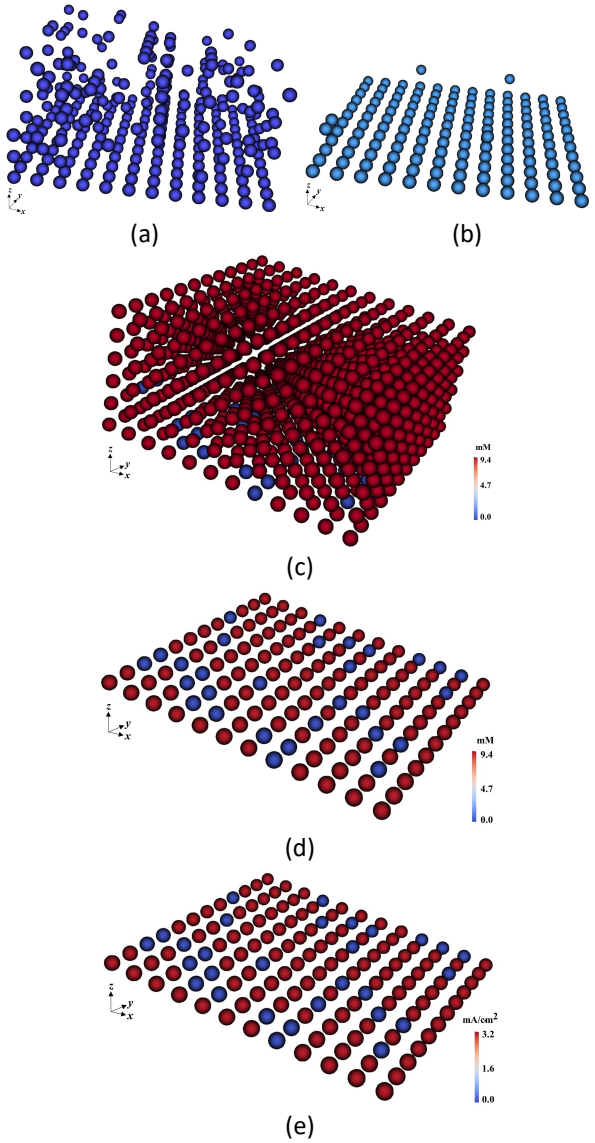

Fig. 3 The distributions of (a) hydrophilic pore; (b) liquid pore; (c) oxygen concentration inside the porous GDL; (d) oxygen concentration and (e) photocurrent density in the photocatalytic pores.

The transport characteristics of multiple species inside the thin porous PL are presented in Fig. 4. Fig. 4a and Fig. 4b display the density distributions of electron and hole along the porous PL. The electrons coming from the external circuit are combined with the photo-excited holes at the air-breathing cathode [28]. Therefore, the photo-excited holes transport from the E/P interface to the P/S interface. Moreover, the photocathode is illuminated from the E/P interface. The closer to the E/P interface, the higher the light intensity. More holes can be photo-excited at this side. These two main reasons

result in a continuous decrease of the hole density from the E/P interface to the P/S interface. While the density distribution of electron is mainly dependent on the distribution of the light intensity. As stated early, the illumination comes from the E/P interface. Most photons are absorbed in this region, resulting in a large electron density. Besides, due to the intense absorption by CuO, the photon flux decreases rapidly along the thin porous PL. As a result, the generation of photo-excited electron decreases sharply, leading to the decrease of the electron density from the E/P interface to the P/S interface. As the photocurrent increases, more holes transport to the P/S interface to combine with the electrons from the external circuit, requiring a larger gradient of the hole density. In the meantime, the increased photocurrent implies a negative shift of the photocathode potential. This also contributes to the significant decrease of the hole density at the P/S interface, making thereby the hole density decreases with increasing the photocurrent, as shown in Fig. 4b. The reduced hole density decreases the recombination rate of the photo-excited holes and electrons at the air-breathing photocathode. As a result, although an increase in the photocurrent results in more photo-electrons to be consumed for the photoelectrochemical reaction of oxygen reduction, the electron density still increases with increasing the photocurrent, as shown in Fig. 4a. This result is also in accordance with the accelerated photoelectrochemical reduction rate at a higher electron density.

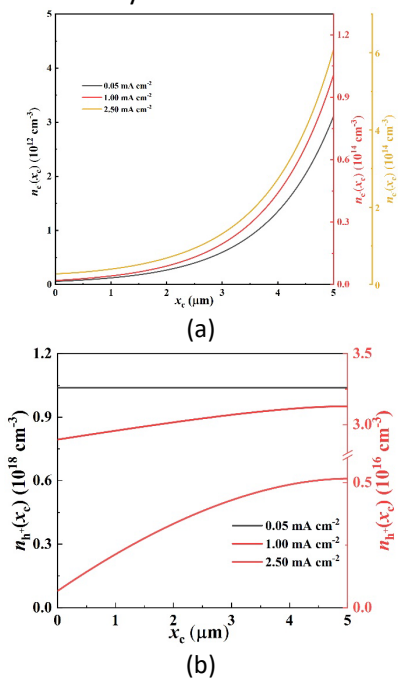

Fig. 4 The distributions of (a) electron density; (b) hole density along the thin porous PL.

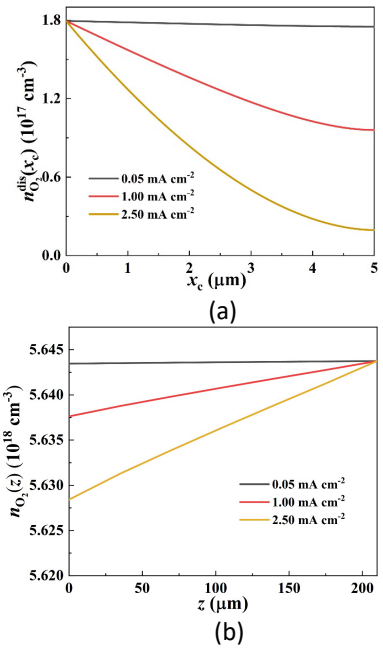

Fig. 5 The distributions of (a) dissolved oxygen concentration along the thin porous PL; (b) oxygen concentration along the porous GDL.

Fig. 5a and Fig. 5b display the distributions of the dissolved oxygen concentration along the thin porous PL and oxygen concentration along the porous GDL. Resulting from the oxygen consumption by the photoelectrochemical reactions, oxygen diffuses from the surrounding through the porous GDL to the thin porous PL. The oxygen concentration decreases along the porous GDL and the dissolved oxygen concentration decreases along the thin porous PL. The larger the photocurrent, the more the consumption of dissolved oxygen due to the photoelectrochemical reduction reactions. To ensure the oxygen transport, the decrease of the gaseous oxygen concentration and dissolved oxygen concentration becomes more obvious. However, fast diffusion of the gaseous oxygen and low liquid saturation result in the inconspicuous decrease of the gaseous oxygen concentration along the porous GDL. While for the dissolved oxygen, it is almost depleted near the E/P interface when the photocurrent density increases to 2.5 mA/cm^2. The sluggish transport of the dissolved oxygen is a limiting factor to the air-breathing photocathode performance.

3.2 Effect of mixed wettability of GDL

The porous GDL usually has a mixed wettability, which makes great significance on the liquid electrolyte percolation, and thus the oxygen transport and the performance. Therefore, the effect of mixed wettability of the porous GDL is discussed in this section. Except the proportion of hydrophilic pores/throats varies from 0.1 to 0.4, the other conditions are the same as the ones

used in the section 3.1. Apparently, more interconnected hydrophilic pores exist when the proportion of hydrophilic pores/throats increases, which promotes the liquid electrolyte percolation into the porous GDL. As a result, more hydrophilic pores are invaded by the liquid electrolyte (Fig. 6a), leading to a higher liquid saturation (Fig. 6b). As the liquid saturation increases, the transport of oxygen in the porous GDL is resisted. However, it should be noted that the photoelectrochemical reactions occurring in the photocatalytic pores fully surrounded with the liquid electrolyte are assumed to be neglected due to critically high mass transfer resistance of dissolved oxygen (Fig. 3d and 3e). In this case, more photocatalytic pores located at the bottom of the constructed 3D pore network are enveloped by the liquid pores and liquid throats, lowering the air-breathing photocathode performance (Fig. 6c). At a given potential, the lowered photocathode performance causes the oxygen consumption rate to decrease, represented by the reduction in the photocurrent density. Therefore, although the increase of the liquid saturation resists the transport of oxygen in the porous GDL, the oxygen concentration is still increased due to the decreased oxygen consumption rate (Fig. 7).

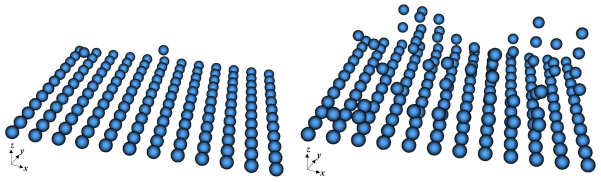

(a)

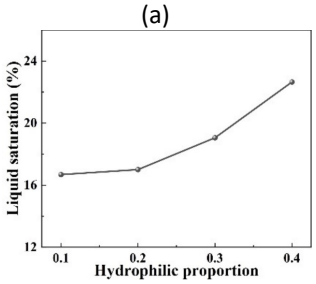

(b)

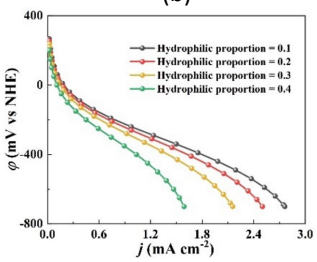

(c)

Fig. 6 Effect of mixed wettability on (a) the distributions of liquid pore (left: hydrophilic proportion = 0.1; right: hydrophilic proportion = 0.4) and (b) liquid saturation inside the porous GDL; (c) the photocathode performance.

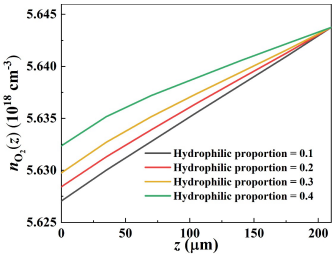

Fig. 7 Effect of mixed wettability on the distributions of oxygen concentration along the porous GDL.

4. CONCLUSIONS

In this work, a pore network model is proposed for the air-breathing CuO photocathode employed in a photocatalytic fuel cell, in which the two-phase percolation in the porous gas diffusion layer and multi-species transport coupled with the photoelectrochemical oxygen reduction reaction in the porous photocatalytic layer are considered. With the proposed model, the two-phase and multi-species transport characteristics for the air-breathing photocathode are systemically discussed. It is demonstrated that the hydrophobic treatment can effectively prevent liquid invasion and promote oxygen transport. The transport of dissolved oxygen and electron/hole greatly affects the photoelectrochemical reaction rate and thereby the photocathode performance. Effects of the mixed wettability of the porous gas diffusion layer are also studied. It is shown that the increase of the proportion of hydrophilic pores/throats in the gas diffusion layer greatly lowers the photocathode performance due to more severe liquid invasion. The present work not only reveals the multi-phase and multi-species transport characteristics in the air-breathing photocathode, but also provides a theoretical foundation for the design of the air-breathing photocathode.

ACKNOWLEDGEMENT

The authors gratefully acknowledge the financial supports of the National Natural Science Foundation of China (No. 51925601) and Innovative Research Group Project of National Natural Science Foundation of China (No. 52021004).

DECLARATION OF INTEREST STATEMENT

The authors declare that they have no known competing financial interests or personal relationships that could have appeared to influence the work reported in this paper. All authors read and approved the final manuscript.

REFERENCE

[1] Li K, Xu Y, He Y, Yang C, Wang Y, Jia J. Photocatalytic fuel cell (PFC) and dye self-photosensitization photocatalytic fuel cell (DSPFC) with BiOCl/Ti photoanode under UV and visible light irradiation. Environ. Sci. Technol. 2013;47(7):3490-7.

[2] Antoniadou M, Kondarides DI, Labou D, Neophytides S, Lianos P, An efficient photoelectrochemical cell functioning in the presence of organic wastes. Sol. Energy Mater. Sol. Cells 2010;94(3): 592-7.

[3] Panah SM, Moakhar RS, Tan HR, Wong TI, Chi D, Dalapati GK. Nanocrystal engineering of sputter grown CuO photocathode for visible light driven electrochemical water splitting. ACS Appl. Mater. Interfaces 2016;8(2):1206-13.

[4] Kushwaha A, Moakhar RS, Goha GKL, Dalapatia GK. Morphologically tailored CuO photocathode using aqueous solution technique for enhanced visible light driven water splitting. J. Photochem. Photobiol. A-Chem. 2017;337:54-61.

[5] Y. Liu, L. Liu, F. Yang, Energy-efficient degradation of rhodamine B in a LED illuminated photocatalytic fuel cell with anodic Ag/AgCl/GO and cathodic ZnIn2S4 catalysts, Rsc Adv. 6 (2016) 12068.

[6] Liu J, Xia M, Chen R, Zhu X, Liao Q, Ye D, Zhang B, Zhang W, Yu Y. A membrane-less visible-light responsive micro photocatalytic fuel cell with the laterally-arranged CdS/ZnS-TiO_2 photoanode and air-breathing CuO photocathode for simultaneous wastewater treatment and electricity generation. Sep. Purif. Technol. 2019;229:115821.

[7] Wang Y, Leung DYC. Toward the scaling up of microfluidic fuel cells, investigation and optimization of the aggravated cathode flooding problem. Electrochim. Acta 2016;222: 312-22.

[8] Rebai M, Prat M. Scale effect and two-phase flow in a thin hydrophobic porous layer. Application to water transport in gas diffusion layers of proton exchange membrane fuel cells. J. Power Sources 2009;192(2):534-43.

[9] Chen L, Zhang R, He P, Kang Q, He YL, Tao WQ. Nanoscale simulation of local gas transport in catalyst layers of proton exchange membrane fuel cells. J. Power Sources 2018;400:114-25.

[10] Niblett D, Mularczyk A, Niasar V, Eller J, Holmes S. Two-phase flow dynamics in a gas diffusion layer - gas channel - microporous layer system. J. Power Sources 2020;471: 228427.

[11] Wu R, Zhao CY, Tsotsas E, Kharaghani A. Convective drying in thin hydrophobic porous media. Int. J. Heat Mass Transf. 2017;112:630-42.

[12] Sinha PK, Wang CY. Pore-network modeling of liquid water transport in gas diffusion layer of a polymer electrolyte fuel cell. Electrochim. Acta 2007;52(28):7936-45.

[13] Zhang W. Pore-scale modeling of the two-phase flow, transport and reaction in porous electrode of air-breathing microfluidic fuel cells with flow-through anode. M.S. thesis. Chongqing University; 2021.

[14] Kemppainen E, Halme J, Lund P. Physical modeling of photoelectrochemical hydrogen production devices. J. Phys. Chem. C 2015;119(38): 21747–66.

[15] Nelson J, Chandler RE. Random walk models of charge transfer and transport in dye sensitized systems. Coord. Chem. Rev. 2004;248(13-14):1181-94.

[16] Gostick JT, Ioannidis MA, Fowler MW, Pritzker MD. Pore network modeling of fibrous gas diffusion layers for polymer electrolyte membrane fuel cells. J. Power Sources 2017;173(1): 277-90.

[17] Wu R, Liao Q, Zhu X, Wang H. Impacts of the mixed wettability on liquid water and reactant gas transport through the gas diffusion layer of proton exchange membrane fuel cells. Int. J. Heat Mass Transf. 2012;55(9-10):2581-9.

[18] Moein-Jahromi M, Movahed MS, Kermani MJ. Numerical study of the cathode electrode in the Microfluidic Fuel Cell using agglomerate model. J. Power Sources 2015;277:180-92.

[19] Gaudy YK, Haussener S. Utilizing modeling, experiments, and statistics for the analysis of water-splitting photoelectrodes. J. Mater. Chem. A 2016;4(8):3100–14.

[20] Trotochaud L, Mills TJ, Boettcher SW. An optocatalytic model for semiconductor catalyst water-splitting photoelectrodes based on in situ optical measurements on operational catalysts. J Phys Chem Lett 2013;4(6):931–5.

[21] Figueiredo V, Pinto JV, Deuermeier J, Barros R, Alves E, Martins R, Fortunato E. P-type Cu_xO thin-film transistors produced by thermal oxidation. J. Disp. Technol. 2013;9(9): 735-40.

[22] Jundale DM, Joshi PB, Sen S, Patil VB. Nanocrystalline CuO thin films: synthesis, microstructural and optoelectronic properties. J. Mater. Sci.-Mater. Electron. 2012;23(8):1492-9.

[23] Wang H, Leung DYC, Xuan J. Modeling of an air cathode for microfluidic fuel cells: Transport and polarization behaviors. Electrochem. Solid State Lett. 2011;36(22):14704-18.

[24] Moein-Jahromi M, Movahed S, Kermani MJ. Numerical study of the cathode electrode in the

Microfluidic Fuel Cell using agglomerate model. J. Power Sources 2015;277:180-92.
[25] Würfel, P. Physics of solar cells: from principles to new concepts. Weinheim: Wiley-VCH;2005.
[26] Vikraman D, Park HJ, Kim SI, Thaiyan M. Magnetic, structural and optical behavior of cupric oxide layers for solar cells. J. Alloy. Compd. 2016;686:616-27.
[27] Zhang Q, Zhang K, Xu D, Yang G, Huang H, Nie F, Liu C, Yang S. CuO nanostructures: Synthesis, characterization, growth mechanisms, fundamental properties, and applications. Prog. Mater. Sci. 2014;60:208-337.
[28] Wu Z, Zhao G, Zhang Y, Liu J, Zhang YN, Shi H. A solar-driven photocatalytic fuel cell with dual photoelectrode for simultaneous wastewater treatment and hydrogen production. J. Mater. Chem. A 2015;3(7):3416-24.